Regional Maximum Entropy Theory of Vortex Crystal Formation

D. Z. Jin and Daniel H. E. Dubin

Physics Department, University of California at San Diego, La Jolla, California 92093
(Received 29 September 1997)

Experiments on pure electron plasmas have found that the decay of 2D turbulence can lead to spontaneous formation of "vortex crystals," which are symmetric arrays of strong vortices within a background of weaker vorticity. In this paper we show that these vortex crystals can be described as regional maximum fluid entropy states. The theory explains the observed patterns of the vortex crystals as well as the vorticity distribution of the background. [S0031-9007(98)06133-X]

The free relaxation of turbulence in inviscid, incompressible 2D fluids is an active area of research, with applications to geophysical and astrophysical flows. The evolution of these fluids is described by the 2D Euler equation $\partial_t \omega + \mathbf{v} \cdot \nabla \omega = 0$, where $\omega(\mathbf{r}, t) = \hat{\mathbf{z}} \cdot \nabla \times \mathbf{v}(\mathbf{r}, t)$ is the vorticity of the flow, and $\hat{\mathbf{z}}$ is a unit vector normal to the plane of the flow. The stream function $\psi(\mathbf{r}, t)$ determines the velocity by $\mathbf{v} = \nabla \times \psi \hat{\mathbf{z}}$, and is related to the vorticity via the Poisson's equation

$$\nabla^2 \psi = -\omega . \tag{1}$$

In recent years, two competing theories have been proposed to describe the free relaxation of 2D turbulence. One is the global maximum fluid entropy (GMFE) theory [1], which states that the turbulent flow can be thought of as a collection of nonoverlapping, incompressible microscopic vorticity elements that become ergodically mixed in the relaxed state. The other theory is the punctuated scaling theory (PST) [2], which states that the turbulent flow is dominated by well separated strong vortices (intense patches of vorticity), whose dynamics can be described by the Hamiltonian dynamics of point vortices punctuated by occasional mergers of like sign strong vortices.

However, neither of these theories provides a complete description for all 2D turbulent flows. This is clearly demonstrated by the recent experimental discovery of "vortex crystals" in a magnetized pure electron plasma column. The electrons evolve as a nearly inviscid, incompressible 2D Euler flow in a circular domain with a free-slip boundary, with the unusual characteristic of a single sign of vorticity, giving a nonzero total circulation. Initial conditions are chosen so that strong vortices form due to a Kelvin-Helmholtz instability. The strong vortices move chaotically due to mutual advection, resulting in pairwise merger events and the formation of filamentary structures. These filaments are mixed by the flow, forming a low vorticity background. This turbulent flow then relaxes spontaneously to a vortex crystal equilibrium, in which a number of strong vortices remain and form a stable pattern in the low vorticity background. The pattern persists for 10^4 turnover times of the column, until dissipation effects destroy the individual strong vortices [3]. Several experimental images of the vortex crystals are displayed in the top row of Fig. 1.

Clearly, the GMFE theory cannot explain the vortex crystals, since the theory predicts a smooth vorticity distribution without strong vortices [1]. On the other hand, the PST predicts a power law decrease over time of the number of strong vortices [2]. This agrees with the early evolution of the experimental flow [3], but the theory does not explain why several strong vortices
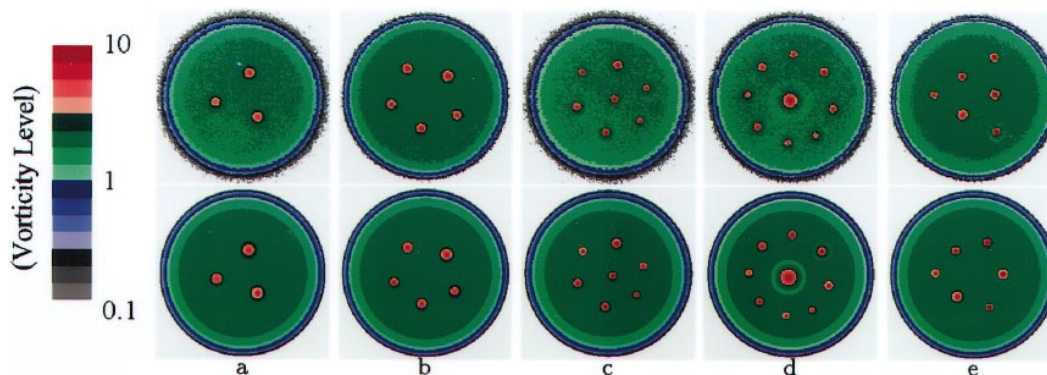

FIG. 1(color). Top: examples of experimental images of vortex crystal states (taken from Ref. [3]). Bottom: corresponding regional maximum fluid entropy states. False color contour plots of vorticity are displayed.

remain and fall into an equilibrium pattern in the final state of the turbulent relaxation.

In this paper we propose that these two theories should work together to describe turbulent flows like those leading to the formation of vortex crystals. The key idea is to recognize that some regions of the flow are well mixed, while other regions are not. The strong vortices ergodically mix the background, driving it into a state of maximum fluid entropy. This mixing, in return, affects the punctuated dynamics of the strong vortices, "cooling" their chaotic motions, and driving them into an equilibrium pattern. However, the vorticity in the strong vortices is trapped and remains unmixed. The resulting equilibrium is called a "regional" maximum fluid entropy (RMFE) state, in order to distinguish it from the GMFE state that allows no unmixed regions and hence no strong vortices. In the rest of the paper, we first characterize the RMFE states, and then show that the vortex crystal states are well described by RMFE theory. Detailed aspects of the theory will be presented in a forthcoming paper [4].

The quantities that determine the RMFE state include the conserved quantities of the flow that survive coarse graining: the (nonzero) total circulation $\Gamma = \int d\mathbf{r}^2 \omega$, the angular momentum $L = -\int d\mathbf{r}^2 \, \omega r^2/2$ (conserved since the flow is bounded by a free-slip circular boundary), and the energy $H = \int d\mathbf{r}^2 |\mathbf{v}|^2/2 = \int d\mathbf{r}^2 \psi \omega/2$. Also, the vorticity levels of the microscopic vorticity elements making up the background must be specified.

In addition to the above quantities, we need to know the number M of the surviving strong vortices and the vorticity distribution in each of them. These properties of the strong vortices depend on the details of the early evolution of the flow, and lie beyond the scope of our statistical theory. Here we focus on the evolution of the flow after mergers of the strong vortices have ceased. Then two properties of the flow can be predicted based on the RMFE theory: the coarse-grained vorticity distribution of the background $\omega_b(\mathbf{r})$, and the equilibrium positions of the strong vortices $\mathbf{R}_i, i = 1, \ldots, M$.

The equations that characterize the RMFE states are obtained by maximizing the fluid entropy $S[\omega_b(\mathbf{r})]$ associated with the coarse-grained background vorticity distribution $\omega_b(\mathbf{r})$. The entropy can be calculated by counting the number of ways of arranging microscopic vorticity elements to obtain the given coarse-grained vorticity. For the simplest case of vorticity elements all having the same positive vorticity ω_f, the entropy is [1] $S[\omega_b(\mathbf{r})] = -\int d\mathbf{r}^2 \{p(\mathbf{r}) \ln p(\mathbf{r}) + [1 - p(\mathbf{r})]\ln[1 - p(\mathbf{r})]\}$, where $p(\mathbf{r}) \equiv \omega_b(\mathbf{r})/\omega_f$. The second term is due to the incompressibility of the vorticity elements, and does not appear in the usual (Boltzmann) expression of the entropy for a compressible flow.

The maximization of S while keeping H, L, and Γ constant is done by finding the extrema of $S' \equiv S - \beta(H - \Omega L + \mu\Gamma)$ with respect to the independent variables $\{\mathbf{R}_i\}$ and $\omega_b(\mathbf{r})$ [5]. Here β, Ω, and μ are Lagrange multipliers that can be interpreted as inverse "temperature," rotation frequency, and the chemical potential, respectively. The extrema of S' with respect to $\{\mathbf{R}_i\}$ are given by

$$\frac{\partial S'}{\partial \mathbf{R}_i} = \frac{\partial}{\partial \mathbf{R}_i}(H - \Omega L) = 0. \tag{2}$$

Since $H - \Omega L$ is the Hamiltonian of the system in a frame rotating at frequency Ω, Eq. (2) shows that in the RMFE state the velocities of the strong vortices are zero in this rotating frame; in other words, the strong vortices are in equilibrium, rotating rigidly at frequency Ω.

The extremum of S' with respect to $\omega_b(\mathbf{r})$ is given by $\delta S' = 0$, i.e., $\int d\mathbf{r}^2 \{\ln p(\mathbf{r}) - \ln[1 - p(\mathbf{r})] + \beta\omega_f\phi\} \times \delta\omega_b(\mathbf{r}) = 0$ for small, arbitrary $\delta\omega_b(\mathbf{r})$, where $\phi \equiv \psi + \frac{1}{2}\Omega r^2 + \mu$ is the stream function in the rotating frame. Therefore,

$$\omega_b(\mathbf{r}) = \omega_f/(e^{\beta\omega_f\phi} + 1). \tag{3}$$

This is very similar to the Fermi distribution in quantum statistics, which is not unexpected since the microscopic vorticity elements are incompressible.

Equations (2) and (3) characterize the RMFE states, and contain vortex crystal solutions. This is illustrated for zero temperature ($\beta \to +\infty$). In this case, there are two types of solutions. One is a shear-free (Boltzmann) equilibrium with $\phi = 0$ in the background, and the other solution is a Fermi-degenerate equilibrium with $\phi = 0$ only on the boundaries of the background (inside the background $\phi < 0$, and outside $\phi > 0$). Which solutions one obtains depends on the values of the conserved quantities [4].

For the Boltzmann equilibrium, Eq. (3) implies that $\omega_b(\mathbf{r})$ is constant within the background, and is less than ω_f. Also, since $\phi = 0$ in the background, every strong vortex is completely shielded by a circular "hole," which is a circular region that excludes the background with radius chosen so that the average vorticity of the strong vortex taken over the hole equals the background vorticity. The strong vortices can take arbitrary (but nonoverlapping) positions, so no vortex crystal state forms in this case. This is also the only type of solution at zero temperature if the Boltzmann distribution, rather than Eq. (3), is used.

For the Fermi degenerate equilibrium, Eq. (3) implies $\omega_b(\mathbf{r}) = \omega_f$ in the background. As opposed to the Boltzmann equilibrium, the strong vortices are now either partially shielded or unshielded. This can be understood from the following argument. When the radius of a strong vortex is small, $\phi > 0$ on its boundary because the contribution to ϕ from the strong vortex is positive and large. Since $\phi < 0$ in the background, a hole must therefore form around the strong vortex. However, the hole cannot cancel out the influence of the strong vortex, because ϕ changes from positive to negative across the hole boundary, implying a finite $\nabla\phi$ exists within the background. Furthermore, when the radius of a strong vortex is sufficiently large, it is possible that $\phi < 0$

on the boundary of the strong vortex. In this case no shielding hole forms around the strong vortex, and the vortex is completely unshielded. Since the vortices are not shielded from each other, Eq. (2) implies that their interaction sets up a vortex crystal state. The size of the crystal is determined from Eq. (2) by a balance between the repulsive force between the strong vortices and the rotational "pseudopotential" force arising from angular momentum conservation.

We now show that the observed vortex crystals are well described by RMFE states. From an experimental flow, we first determine the number M of strong vortices by counting the clumps with local vorticity extrema much larger than the average vorticity of the flow [6]. Next, the vorticity distribution in the ith strong vortex is specified by the vorticity radial profile $\zeta_i(|\mathbf{r} - \mathbf{R}_i|)$ around the local extremum. The vorticity profile (rather than merely the circulation) of each strong vortex is required because the self-energy of the strong vortex must be included in H.

In order to completely specify the problem, we must choose a value for the Fermi vorticity ω_f associated with the vorticity elements of the background. In fact, the general theory [1] allows for a distribution of values for ω_f, but we have found that a single value is sufficient to explain the experiments. The value of ω_f is determined by the following two considerations: (i) ω_f must be larger than or equal to the maximum observed background vorticity level, which is coarse grained by the experimental imaging system; (ii) since the observed vortex crystal states appear to be nearly Fermi degenerate, in some finite region of the background the coarse-grained vorticity should approach ω_f. We therefore take $\omega_f = \omega_{\max}$, where $\omega_{\max}$ is the maximum of the observed background vorticity. Furthermore, we find that all of the observed vortex crystal states have $\omega_{\max} = 2.15 \pm 0.05$, apparently because their initial conditions are similar. Therefore, $\omega_f = 2.15$ is used in all of our calculations. Lengths are scaled by r_w (the radius of the circular free-slip boundary), and vorticities are scaled by Γ/r_w^2.

Along with ω_f and ζ_i, we also evaluate the conserved quantities H, L, and Γ from the experimental flow using their previous definitions. These inputs from the experimental flow determine the corresponding RMFE state with no free parameters. For fixed ω_f and ζ_i we numerically search for the proper values of β, Ω, and μ needed to match the experimental values of H, L, and Γ.

Specifically, for given values of β, Ω, μ, and the positions of the strong vortices $\{\mathbf{R}_i\}$, the stream function ψ and the background vorticity ω_b are found by solving Eqs. (1) and (3) using the FAS algorithm [7] on 513×513 uniform grids. The relative error of the solution is of order 10^{-4}. The positions $\{\mathbf{R}_i\}$ are then varied using Broyden's method [7] and ψ and ω_b are recalculated until the force-balance criteria, Eq. (2), are satisfied. The initial guess for the positions of the strong vortices is taken from the experimental flow. Parameters β, Ω, and μ are varied using Broyden's method until the correct values of H, L, and Γ are obtained. Solutions for β, Ω, μ, and $\{\mathbf{R}_i\}$ converge within a relative error of order 10^{-2}.

The RMFE solutions reproduce the observed vortex crystal patterns, as shown in Fig. 1. Also, the observed background vorticity is close to the theory, as can be seen in the θ-averaged vorticity profiles of Fig. 2. The background of these finite temperature solutions has the following features: the edge falls off gradually, since the vorticity elements near the edge can fluctuate in energy by an amount of order $1/\beta$; also, near a strong vortex the background vorticity is slightly depressed, since ϕ tends to increase due to the influence of the strong vortex, as can be observed around the large central vortex in Fig. 1(d).

Some of the patterns appear to agree more closely with the theory than others. There are two natural ways of quantitatively measuring this accuracy: the deviation of the crystal geometry and the deviation of the background vorticity. The geometry deviation G is defined as $G^2 = \sum_{i \neq j}(d_{ij}^{\exp} - d_{ij}^{\text{th}})^2/M(M-1)$, where $d_{ij}^{\exp}$ and d_{ij}^{th} are the distances between the ith and the jth strong vortices in experiment and in theory, respectively. The background deviation B is defined as $B^2 = \int d\mathbf{r}^2\, \omega_b(\mathbf{r})[\omega_b^{\exp}(\mathbf{r}) - \omega_b(\mathbf{r})]^2/\int d\mathbf{r}^2\, \omega_b(\mathbf{r})$, where $\omega_b^{\exp}(\mathbf{r})$ and $\omega_b(\mathbf{r})$ are the vorticity distribution of the background in experiment and in theory, respectively. Here the region of integration
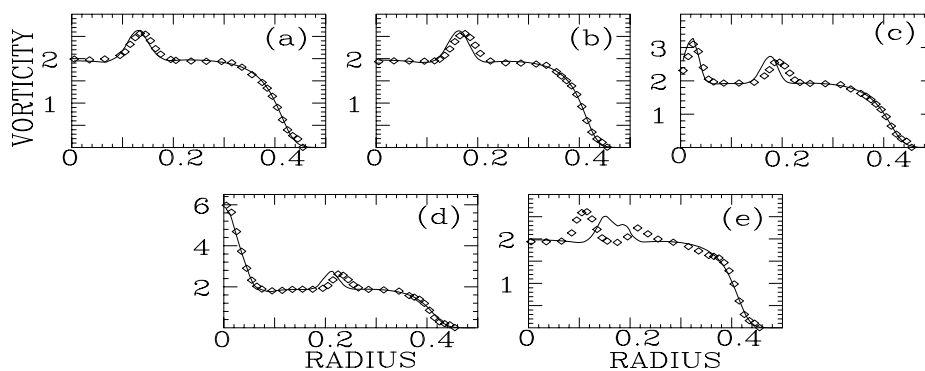

FIG. 2. Comparison between theory (solid line) and experiment (symbol ◇) for the θ-averaged vorticity profiles of the vortex crystal states in Fig. 1.
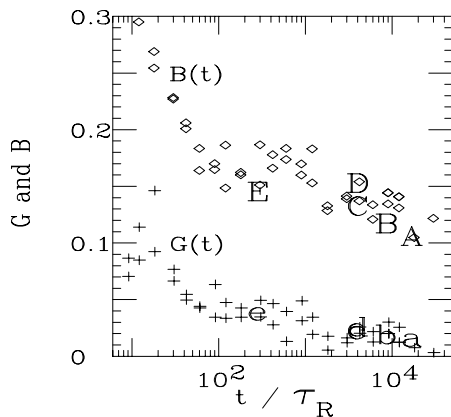
FIG. 3. The evolution of the geometry deviation G (symbol $+$) and the background deviation B (symbol $\diamond$) for the flow discussed in Ref. [1]. Symbols a,b,c,d,e (for geometry deviations), and A,B,C,D,E (for background deviations) correspond to the states shown in Fig. 1.

excludes regions occupied by the strong vortices both in experiment and in theory. The average is weighted by $\omega_b(\mathbf{r})$ in order to reduce the experimental noise from the regions of low vorticity.

The values of these deviations for the vortex crystals displayed in Figs. 1 and 2 are indicated in Fig. 3 at the times when the patterns were observed. Here $\tau_R = 170\ \mu$s is the bulk rotation time of the fluid as in Ref. [3]. The deviations in Figs. 1(e) and 2(e) are relatively large. We argue that this is because these data were taken at an early time, and the flow has not yet settled into the RMFE state. To justify this claim, we have analyzed the time evolution of the flow that led to vortex crystals discussed in Ref. [3]. For each experimental image of this flow after strong vortices have formed, geometry and background deviations from the corresponding RMFE state were calculated. The results are shown in Fig. 3, which clearly show that the deviations decrease as time elapses. The dynamics leads the system towards RMFE states.

In conclusion, the following physical picture of vortex crystal formation emerges from our analysis: an initially unstable vorticity profile breaks up into many strong vortices. While these strong vortices undergo chaotic mergers described by the PST, they also ergodically mix the low vorticity background. The mixing of the background, in return, cools the chaotic motions of the strong vortices, and drives the strong vortices into a vortex crystal equilibrium. This picture shows that the interaction between the

strong vortices and the background, a process neglected in the PST, can be important in understanding the relaxation of 2D turbulence. It also shows that fluid entropy maximization can provide useful results for the relaxed state [8], provided that one recognizes that in general only certain parts of the flow may be well mixed.

However, there are questions that remain to be answered. In the paper we have assumed that the microscopic vorticity elements have the same vorticity level ω_f. It is important to understand why this simple assumption works so well. Also, the dynamics of the background mixing and the rate at which the strong vortices relax to the equilibrium patterns should be investigated.

[1] J. Miller, Phys. Rev. Lett. **65**, 2137 (1990); R. Robert and J. Sommeria, J. Fluid Mech. **229**, 291 (1991); J. Miller, P. B. Weichman, and M. C. Cross, Phys. Rev. A **45**, 2328 (1992), and references therein.

[2] G. F. Carnevale *et al.,* Phys. Rev. Lett. **66**, 2735 (1991); J. B. Weiss and J. C. McWilliams, Phys. Fluids A **5**, 608 (1993).

[3] K. S. Fine, A. C. Cass, W. G. Flynn, and C. F. Driscoll, Phys. Rev. Lett. **75**, 3277 (1995).

[4] D. Z. Jin and D. H. E. Dubin (to be published).

[5] The extrema of S' can be maxima, saddle points, or minima. To ensure that S is maximized under the constraints, the second variation of S' must be negative. We will discuss this issue in Ref. [4].

[6] J. C. McWilliams, J. Fluid Mech. **219**, 361 (1990).

[7] W. H. Press *et al., Numerical Recipes in Fortran* (Cambridge University, Cambridge, England, 1992).

[8] Other variational principles, such as maximization of Boltzmann entropy [see, for example, R. A. Smith, Phys. Rev. A **43**, 1126 (1991); D. Montgomery *et al.,* Phys. Fluids A **5**, 2207 (1993)] or minimization of enstrophy [see C. Leith, Phys. Fluids **27**, 1388 (1984)], have also been employed to understand the decay of 2D turbulence. For a review, see M. Brown, J. Plasma Phys. **57**, 203 (1997). However, these principles cannot be applied to explain the vortex crystal data of Figs. 1 and 2, and hence are not discussed here. For details, see Ref. [4].